Título artículo / Títol article:	Atmospheric plasma spraying coatings from alumina–titania feedstock comprising bimodal particle size distributions.
Autores / Autors	Vicent, Mónica ; Bannier, Emilie ; Moreno, Rodrigo ; Salvador Moya, María Dolores ; Sánchez Vilches, Enrique Javier
Revista:	Journal of the European Ceramic Society
Versión / Versió:	Pre-print
Cita bibliográfica / Cita bibliogràfica (ISO 690):	VICENT, Mónica, et al. Atmospheric plasma spraying coatings from alumina–titania feedstock comprising bimodal particle size distributions. Journal of the European Ceramic Society, 2013, vol. 33, no 15, p. 3313-3324.
url Repositori UJI:	http://hdl.handle.net/10234/96395

Atmospheric plasma spraying coatings from alumina-titania feedstock comprising bimodal particle size distributions

Mónica Vicent [(1)], Emilie Bannier [(1)], Rodrigo Moreno [(2)], Mª Dolores Salvador [(3)], Enrique Sánchez [(1)]

[(1)] Instituto de Tecnología Cerámica (ITC), Asociación de Investigación de las Industrias Cerámicas (AICE), Universitat Jaume I (UJI), Castellón, Spain.

[(2)] Instituto de Cerámica y Vidrio (ICV), Consejo Superior de Investigaciones Científicas (CSIC), Madrid, Spain.

[(3)] Instituto de Tecnología de Materiales (ITM), Universidad Politécnica de Valencia (UPV), Valencia, Spain.

List of all authors and their affiliations:

Mónica Vicent Cabedo [(1)]

Emilie Marie Bannier [(1)]

Rodrigo Moreno Botella [(2)]

Mª Dolores Salvador Moya [(3)]

Enrique Sánchez Vilches [(1)]

Full contact details for the corresponding author:

Mónica Vicent Cabedo

Instituto de Tecnología Cerámica (ITC)

Campus Universitario Riu Sec | Av. Vicent Sos Baynat s/n | 12006 Castellón (Spain)

T. +34 964 34 24 24 | F. +34 964 34 24 25 | www.itc.uji.es

monica.vicent@itc.uji.es

Abstract

In this work, Al_2O_3-13 wt% TiO_2 submicron-nanostructured powders were deposited using atmospheric plasma spraying. The feedstocks were obtained by spray drying two starting suspensions of different solids content, prepared by adding nanosized TiO_2 and submicron-sized Al_2O_3 powders to water. The spray-dried granules were heat-treated to reduce their porosity and the powders were fully characterised in both untreated and thermally treated state. Comparison with two commercial feedstocks was carried out. Characterisation allowed a temperature for the thermal treatment to be chosen on the basis of the sprayability of the feedstock and the preservation as much as possible of the submicron-sized structure of the unfired agglomerates.

Optimisation of the deposition conditions enabled the reconstituted powders to be successfully deposited, yielding coatings that were well bonded to the substrate. The coating microstructure, characterised by SEM, was mostly formed by a matrix of fully molten particles where the presence of semi-molten feedstock agglomerates was also observed.

Moreover, microhardness, toughness, adhesion and tribological behaviour were determined, and the impact of the granule characteristics on these properties was studied. It was found that changing the feedstock characteristics allows controlling the coating quality and properties. In general, good mechanical properties were obtained by using a feedstock comprising a binary mixture of submicrometric Al_2O_3 and nanometric TiO_2 particles in the spray-dried powder.

Keywords: Suspensions; Al_2O_3-TiO_2; Nanoparticle; Rheology; Spray-dried powders.

1 Introduction

Thermal spray, and particularly atmospheric plasma spray (APS), is one of the most economical and viable processes to obtain coatings at an industrial scale, given its high deposition rates and that there is no need for special atmospheric or chemical chambers. Additional advantages are the durability and high thickness of the coatings.

The manufacture of nanostructured coatings would provide enhanced properties over those obtained for micronic or submicronic ones. In order to obtain nanostructured coatings it is necessary to use nanoparticles as raw material. However, nanoparticles need to be reconstituted to a sprayable size in order to use regular powder feeders as well as to provide a route to safe handling of nanoparticles [1]. Reconstitution generally takes place by spray drying of a nanoparticle suspension and, frequently, thermal treatment (partial sintering) of the resulting granules [2].

Although many authors have addressed the role of slurry formulation on the characteristics of the ceramic granules and many others have obtained spray-dried powders for thermal spraying [3,4], most papers using nanostructured spray-dried feedstock only mention the agglomeration process without providing a complete experimental study of nanoparticle suspension preparation, spray-drying operation, or thermal treatment of the resulting agglomerates. Thus, the correlation between agglomeration process variables, agglomerate characteristics, and coating microstructure and properties is far from being well established.

Al_2O_3-TiO_2 coatings fabricated with nanopowders show very promising bonding strength and wear resistance when compared with conventional feedstock as reported elsewhere [5,6]. Although, many research effort has been made to pass from the micro-scale to either the nano- or the submicron-scale using both powders or liquids as feedstock [7,8], few attempts have been made to use feedstocks in which mixtures of different particle size distributions, e.g. submicron-nano sized particles. The use of a bimodal distribution of submicron-nano particles, comprising the precursor suspension of the spray-dried powder, can give rise to significant benefits during the suspension processing, i.e higher solids content and lower viscosity leading to better properties in the resulting feedstock agglomerates, such as higher agglomerate bulk density and

improved powder flowability [9,10]. This is particularly interesting for alumina suspension due to the intrinsic difficulties associated with the preparation of concentrated nanoparticle suspensions of alumina as reported elsewhere [11]. The relationship between these improved agglomerate feedstock characteristics and the final coating properties has been scarcely treated in the literature [10]. In this respect, we have also recently reported improved photocatalytic activity in APS TiO_2 coatings when using a mixture of nano and submicrometric particles in the spray-dried feedstock. Much higher density agglomerates were obtained which led to better properties in the final coatings [11,12].

In previous research by the authors, it was found that the nanostructured spray-dried agglomerates obtained from concentrated Al_2O_3-13 wt% TiO_2 suspensions yielded coatings with lower void content than those obtained using powders from less concentrated suspensions [11]. However, feedstocks made up of powders with bimodal particle size distribution (submicronic-nanometric particles) were not explored.

This work deals with the relationship between the reconstituted granule characteristics and the properties of Al_2O_3-13 wt% TiO_2 coatings obtained from spray-dried feedstocks made up of TiO_2 nanoparticles and Al_2O_3 submicrometric particles with a view to addressing the potential benefits of the use of bimodal feedstocks. Complete characterisation of feeding powders (FEG-ESEM, granule size distribution, flowability and apparent density) and of newly developed coatings (microstructure by SEM and mechanical properties such as microhardness, toughness, wear and pull-off) was performed. The expected benefits of the use of submicron sized alumina (instead of nanosized alumina) together with nano sized titania comprising the spray-dried feeedstock can be then summarised as follows: easier suspension preparation and handling with the achievement of much higher solids concentration, better feedstock characteristics associated with an (expected) higher agglomerates density and much lower feedstock cost.

2 Experimental

2.1 Feedstock preparation and characterisation

The following commercial powders were used as starting materials: 1) a submicron-sized, high purity α-Al_2O_3 (Condea-Ceralox HPA-0.5, Sasol, USA) with a mean particle size of 0.35 μm and a specific surface area of 9.5 m^2/g; and 2) a nanosized TiO_2 powder (Aeroxide® P25, Degussa-Evonik, Germany) with an average primary particle size of 40 nm, a specific surface area of 50 m^2/g, and a relative ratio of anatase:rutile phases of 3:1 [13]. Mixtures of submicronic alumina and nanometric titania were always prepared at a relative weight ratio of 87:13. Finally, and for comparison purposes, two commercial feedstocks with the same Al_2O_3:TiO_2 weight ratio, were also deposited: a conventional microstructured one (Metco 130, Sulzer Metco, Germany), referred as MC, and a nanostructured one (Nanox™ S2613S, Inframat Advanced Materials, USA), referred as NC.

The colloidal stability of aqueous suspensions of the TiO_2 nanopowder as well as the coarser alumina powder has been previously evaluated by zeta potential measurements [9]. This information allowed choosing the most adequate nature and proportion of dispersant so as to subsequently prepare high solids content suspensions. Thus concentrated suspensions were prepared to solid contents of 30 vol.% and 50 vol.% (i.e. at 67 and 80 wt%, respectively) using deionised water. A commercial polyacrylic acid-based polyelectrolyte (DURAMAX™ D-3005, Rohm & Haas, USA) was used as a deflocculant. This was supplied as an aqueous solution of polyacrylic acid (PAA) with 35 wt% active matter of PAA [$(C_3H_4O_2)_n$] and an average molecular weight of 2400. Studies elsewhere have shown that this deflocculant is suitable for obtaining concentrated suspensions of both studied materials [13,14]. The suspensions were prepared by adding first the PAA required to disperse all the particles (4 wt% PAA in relation to the titania content and 0.3 wt% PAA in relation to the alumina content). The foregoing PAA contents refer to the active matter concentration. After that, the titania nanopowder was added and homogenized with sonication for 1 min. and subsequently the alumina powder was dispersed (without sonication). The mixture was then kept for 15 min. under mechanical stirring.

It was not necessary to use a binder for spray-drying. In fact, spray-dried granules with adequate mechanical strength were obtained from the 30 vol.% and 50 vol.% suspensions (hereinafter feedstock AsTn30 and AsTn50 respectively) in a spray dryer (Mobile Minor, Gea Niro, Denmark) with a drying capacity of 7 kg water/h as set out elsewhere [11]. Granule size distribution was measured by laser diffraction (Mastersizer, Malvern, UK). Agglomerate apparent density was calculated from powder tapped density by assuming a theoretical packing factor of 0.6, which is characteristic of monosize, spherical particles [15]. Powder flowability was evaluated in terms of the Hausner ratio, determined by dividing powder tapped density by powder apparent density [15]. Free-flowing powders have a Hausner ratio < 1.25.

In order to obtain denser granules, the spray-dried powders were heat treated in an electric kiln at a temperature rate of 25 ºC/min to different maximum temperatures, which depended on the powder sample, with soaking time of 60 minutes [11]. The main objective of the heat treatment is to enhance the mechanical strength of the agglomerates and to reduce their shell porosity meanwhile the submicro/nano-structure of the feedstock agglomerates should be preserved as much as possible [2,11]. A test was previously carried out in a hot stage microscope (Misura 3, Expert System Solutions, Italy) so as to ascertain the temperature of this thermal treatment. The hot stage microscope is an instrument that allows the visualisation of a sample while it is being subjected to a heating cycle. At the same time, it allows the sample shape to be recorded on a computer throughout shrinkage. The recorded images enable the evolution of sample shrinkage to be determined as a function of temperature, by means of an image analysis instrument. The spray-dried sample was used to press a cylindrical button, 3 mm in diameter and 3 mm in height, which was placed on a support that was then set in the hot stage microscope sample holder, where it was subjected to a heating cycle at a rate of 25 °C/min. The shrinkage–temperature curve was determined from the recorded images.

Finally, pore structure was evaluated by mercury intrusion porosimetry, MIP (AutoPore IV 9500, Micromeritics, USA), crystalline phases in feedstock samples were identified by X-ray diffraction technique (XRD D8 Advance, Bruker AXS, Germany) and a field-emission gun environmental scanning electron microscope, FEG-ESEM (QUANTA 200FEG, FEI Company,

USA) was used to examine the microstructure of both untreated and thermally treated feedstocks.

2.2 Coating deposition

Al_2O_3-13 wt% TiO_2 coatings were deposited by APS on stainless steel substrates (AISI 304) prepared as set out elsewhere [16]. The plasma spray system consisted of a gun (F4-MB, Sulzer Metco, Germany) operated by a robot (IRB 1400, ABB, Switzerland). Before spraying, the substrate was blasted with corundum grit and cleaned with ethanol to remove any dust or grease residue from the surface. After that, a Ni–Al metallic alloy (METCO 450NS, Sulzer Metco, Germany) was sprayed between steel substrate and ceramic coating in order to improve adhesion. Moreover, it was also necessary to hold the substrate temperature between 95 ºC and 200 ºC, before Al_2O_3-13 wt% TiO_2 deposition, in order to avoid spalling during the final cooling. Finally, the deposition was made using argon and hydrogen as plasma-forming gases. The same spraying conditions were used in all deposition experiments: Ar flow=35 slpm, H_2 flow=12 slpm, arc intensity=600 A, spraying distance=0.12 m, spraying velocity=1 m/s.

2.3 Coating characterisation techniques

First, the coating microstructures were observed by SEM (JSM6300, JEOL, Japan). Coating porosity was evaluated by image analysis from ten backscattered electron mode micrographs at 1000 magnification. Crystalline phases in coating samples were also identified by X-ray diffraction technique.

The hardness and fracture toughness of the materials were determined using an indentation technique. A conventional diamond pyramid indenter (Vickers) was fit to the piece of equipment (4124, INNOVATEST, Netherlands) and a load of 3 N was applied for 15 s according to the standard specification ASTM E92-72. The fracture toughness was determined by measuring the radial crack length generated on the corners of the track produced as a consequence of the Vickers indentation test. A minimum of 10 tests were averaged for hardness and toughness determination.

Wear tests were carried out under dry sliding conditions using a pin-on-disk tribometer (MT2/60/SCM/T, Microtest, Spain) in accordance with ASTM wear testing standard G99-03.

As friction partner, 5 mm diameter-Si_3N_4 ball was used. The normal load, sliding speed and distance were fixed at 10 N, 0.1 m/s and 1000 m, respectively. Testing was carried out in air, at room temperature. Prior to measuring hardness, toughness and wear, the samples were polished (RotoPol-31, Struers, Denmark) with diamond to 1 µm roughness for hardness and toughness determination, and with SiC to 2-3 µm for wear tests.

The pull-off tests were performed according to ASTM D4541 in a PosiTest (AT-A, DeFelsko, USA). The dolly, whose diameter was 10 mm, was attached to the coating surface with a curable epoxy adhesive for 8 h. After that, the dolly was vertically pulled-off (with a 2.0 MPa/s rate) while measuring the necessary force. The results are the average of 3 repeated tests done on each sample.

3 Results and discussion

3.1 Feed powder agglomeration process

A former study revealed that the conventional powder (MC) is formed by angular particles between 20 and 60 µm obtained by a fusing and crushing process while the nanostructured feedstock (NC) contained highly porous agglomerates with a granule mean size of 38 µm which were made up of nanoparticles with a size ranging 50-500 nm [16]. Figure 1 shows FEG-ESEM micrographs of the as spray-dried powders obtained from 30 vol.% and 50 vol.% suspensions at different magnifications (samples AsTn30 and AsTn50 respectively). The typical doughnut-shape morphology of spray-dried agglomerates is observed in most granules of both powders [11]. However, the 50 vol.% powder shows coarser agglomerates as well as less amount of non-spherical, small agglomerates leading to a more homogeneous powder. This finding coincides with that observed for nanoparticle suspensions obtained with different solids content [11]. Thus, as expected, stable, higher solids content suspensions give rise to larger agglomerates due to the higher suspension viscosity. Higher magnification of the solid areas of the agglomerates of both powders reveals that the granules are porous and formed by the agglomeration of the individual nano and submicron-sized particles. In both powders, coarser alumina particles are clearly visible together with the titania nanoparticles. In addition denser

particle arrangement is observed in the cross section of the AsTn50 powder granule as a result of the much larger number of particles in the stabilised starting suspensions.

Table I lists some properties of interest for spray-dried powders to be used as feedstock in plasma spraying: the Hausner ratio, which is related to the flowability of the powder and the agglomerate bulk density, which is directly related to its weight. Data of reference feedstock (samples MC and NC) are also included. According to literature [3,17], relatively dense (higher than 1000 kg/m^3 apparent density) and free-flowing agglomerates are necessary for a suitable feeding into the plasma torch. In general, all the samples exhibit adequate characteristics to be used as APS powders. However, significant differences can be observed among these four samples (AsTn30, AsTn50, MC and NC). With regard to the agglomerate bulk density although the highest value is shown by the commercial sample MC, this is because this sample is a fused and crushed dense powder. Thus no direct comparison can be done between this feedstock and the corresponding spray-dried powders. The agglomerate density of the two powders obtained in this research is much higher than that of the NC sample as a consequence of the better packing efficiency inside the agglomerate associated with the submicronic-nanometric particle arrangement [12]. Moreover, the Hausner ratio for the three spray-dried powders was ≤ 1.25, indicating good flowability and confirming that they are appropriate for APS process. The higher value of this ratio (lower flowability) for the MC sample is due to the angular morphology of the particles comprising this powder [16]. Note that in the case of as spray-dried powders, granule size distribution could not be measured by laser diffraction as they were broken during the measurement.

3.2 Thermal treatment of the spray-dried powders

Thermal treatment of the spray-dried powders commonly represents the second step of the reconstitution process for feedstock preparation in APS. In order to determine the beginning of the sintering process and thus to determine the heat treatment temperature, tests were conducted in a hot stage microscope. These tests were carried out on powder samples without any preliminary shaping or compaction of the powder and, thus, the results are actually representative of the feed powder behaviour and not of the sintering process of a given shaped

sample or coupon. The evolution of powder shrinkage as a function of temperature is then plotted. Figure 2 shows the shrinkage versus temperature curves for samples AsTn30 and AsTn50 together with the reference NC powder. As expected sample made up of nanoparticles (NC) display much higher sintering rate evaluated from the slope of the shrinkage-temperature curve profile. On contrary the sintering rate of the two other samples is more gradual as a consequence of the presence of submicrometric particle in the powder. Furthermore the role of the agglomerate bulk density (set out in table I) in the sintering process is of paramount significance. On the one hand the higher the agglomerate density the lower the maximum shrinkage. In this way, the maximum sintering shrinkage of NC sample is almost twice that of the two other powders as a consequence of the much lower agglomerate density of the nanostructured feedstock (see table I). On the second hand the decrease of the agglomerate density results in a delay in the initial sintering temperature. This last finding highlights the impact of the agglomerate density on the beginning of the sintering process. Samples made up of bimodal particle size distribution (submicrometric-nanometric sizes), which gave rise to higher agglomerate density (i.e closer particle contact) lead to powders that show lower initial sintering temperatures than those of the NC feedstock despite this last sample is formed by nanoparticles.

Figure 3 shows the FEG-ESEM micrographs of thermally-treated AsTn30 and AsTn50 samples. Similar micrographs for a nanostructured, spray-dried powder were previously reported [11]. The evolution of the agglomerate microstructure is typical of a solid-state sintering process. This sintering process yields significant changes in sizes and shapes of grains and pores. Grain growth for both nano- and submicrometer-sized particles of the starting agglomerates is apparent at 1200 ºC as shown in the micrograph of AsTn30 sample. Thus, the sintering process showed by the shrinkage-temperature curves takes place by means of a rapid grain growth of firstly titania nanoparticles and secondly alumina submicrometric particles [9]. In this way, submicron character of the particles which is visible at 1200 ºC for both powders has practically disappeared at 1235 ºC.

Sintering process can also be followed by monitoring the evolution of the pore structure of the agglomerates. These measurements were directly done on powder sample, not on shaped samples. Pore sizing measurements are particularly intended to analyse the intragranular (fine size) porosity since the powder is fed into plasma torch without any consolidation (shaping) process. Figure 4 shows the pore size distribution curves obtained by mercury intrusion porosimetry for AsTn30 and AsTn50 untreated and thermally treated at 1235 ºC powders. The initial bimodal distribution of porosity is associated with large pores between granules (intergranular porosity, marked INTER in figure 4) and small pores inside the agglomerates (intragranular porosity, marked INTRA in figure 4). The intergranular porosity which largely depends of the sample preparation for porosimetry test shows scarce interest for APS process since the powder is fed into the plasma torch without any compacting effect. But the intragranular porosity allows the sintering effect to be estimated. It is worthwhile noticing that the void associated to the doughnut (toroid) morphology of the spray-dry agglomerates is mainly measured in the first step of Hg intrusion process, i.e where the intergranular porosity is determined. Thus as shown in this figure the initial total porosity (maximum cumulative mercury intrusion volume) and the intragranular pore size (worked out from the INTRA portion of the pore size curve) are smaller for the as-spray-dried AsTn50 powder confirming the higher packing density of the agglomerates obtained from more concentrated suspensions. As the sintering process proceeds, the porosity decreases and the pore size increases as a consequence of the pore coarsening effect of the small pores.

Granule size distribution (Figure 5) confirmed some of the foregoing results. The AsTn50-1200 ºC powder displayed a slightly coarser granule mean size than those of AsTn30-1200 ºC powder. It is generally recognized that thermal spray powders exhibit agglomerate size distributions ranging from 15 to 200 μm [2,18]. The volumetric mean sizes were 57 μm and 110 μm (Table I) and the volumetric quantities of 15 μm undersize agglomerates were only 2.0% and 3.5% for the 30 vol.% and 50 vol.% thermally treated samples, respectively. Thus both powders fit well the average requirements.

As mentioned above the reconstitution process of APS feedstock aims to obtain sprayable, denser agglomerates in which the submicron-sized structure can be as much as possible preserved. As a consequence, the temperature chosen to increase the density was 1200ºC for both AsTn30 and AsTn50 samples (hereinafter AsTn30-1200 ºC and AsTn50-1200 ºC samples respectively). The spray-dried powders were heat treated in an electric kiln with soaking time of 60 minutes at this given temperature. The agglomerate bulk density of the heat treated powders were 3100 kg/m^3 and 3580 kg/m^3 for the samples AsTn30 and AsTn50 respectively (Table I). Despite this partial sintering process, the achieved density values of the thermally treated granules are still lower from those of the MC, fused and crushed grains (3830 kg/m^3). With regard to the Hausner ratio or agglomerate size, the values of these parameters showed almost no variation with temperature (Table I).

Finally, the XRD patterns of the untreated and AsTn30-1200 ºC and AsTn50-1200 ºC samples revealed the following results. As set out in section 2.1, the untreated powder (either AsTn30 or AsTn50) is made up of α-Al_2O_3 and mostly anatase. After heat treating most metastable anatase transforms into stable rutile. α-Al_2O_3 remains as the stable phase for alumina. No formation of aluminium titanate was identified due to the low temperature of the thermal treatment [9]. The patterns of the untreated and thermally treated AsTn50-1200 ºC powders are shown in figure 6. Very similar patterns were obtained with AsTn30 powders.

With regard to reference powders MC and NC, in both cases aluminum oxide was found as corundum (α-Al_2O_3), whereas titanium oxide was mainly composed of anatase with a low proportion of rutile. Concerning the commercial nanostructured powder, XRD analysis also confirmed the presence of some oxide additives (CeO_2 in cerianite form and ZrO_2 as zirconia and baddeleyite) [16].

3.3 Microstructure and phase distribution of the coatings

Four different types of coatings were obtained from the four spray-dried feedstocks (untreated AsTn30 and AsTn50 and heat treated AsTn30-1200 ºC and AsTn50-1200 ºC samples) by depositing all powders according to the spraying conditions set out in section 2.2. This is because the objective of the work was to evaluate the influence of the characteristics of

the different feedstocks on coatings microstructure and properties by keeping constant the (standard) plasma spraying conditions.

Figure 7 shows SEM micrographs at two different magnifications of these four coatings together with two representative micrographs of reference coatings (MC and NC) obtained with the same spraying conditions. The coatings microstructure is clearly influenced by the feedstock characteristics, as revealed by SEM observations (Figure 7). As expected, the coating obtained from the conventional powder (MC) shows a typical splat-like microstructure, formed by successive impacts of fully molten droplets. However, the layers deposited from the nanostructured powder (NC) exhibit a bimodal microstructure formed by partially molten agglomerates that retained the initial nanostructure, surrounded by a fully molten matrix. Such microstructure has been extensively reported in literature [19, 20]. Regarding coatings obtained from untreated and heat treated AsTn30 and AsTn50 samples, these coatings also displayed a few partially molten areas as observed in figure 7, which are made of coarser particles than those comprising the partially molten areas of NC coating, as the feedstock mainly contained submicron particles. Yet, it has to be pointed out that these coatings are mainly formed by fully molten areas, as a consequence of the sintering grade and very low porosity of the initial granules. Thus despite the nanostructured character of the primary particles comprising the commercial NC powder, the high porosity associated to these agglomerates results in coatings containing partially melted areas which preserve in some extent the starting nanostructure. On contrary, the much higher density of the submicrometric-nanometric feedstock diminishes the contribution of the initial agglomerate microstructure to the final coating microstructure. Figure 8 compares higher magnifications micrographs of the partially molten areas in NC and AsTn50-1200 ºC coatings. As it can be seen, partially molten areas in AsTn50-1200 ºC coating are made up of larger particles exhibiting less porous assembly.

The XRD patterns of the coatings are shown in figure 9. Firstly, it can be seen that the coatings obtained from both thermally untreated powders mainly consist of α-Al_2O_3, γ-Al_2O_3 and rutile. These findings are consistent with the phases observed in most of the works related to this Al_2O_3-TiO_2 system which employ submicron or nanostructured feedstocks [18,21].

Secondly, on comparing coatings obtained from thermally treated powders with the coatings made from their corresponding untreated powders the formers display a slightly higher amount of α-Al_2O_3 at the expense of γ-Al_2O_3 which is probably related to the powder trajectory through the plasma torch as well as its melting stage. Finally, some minor phases were also observed, more specifically, there was a little Al_2TiO_5 formed in all the coatings [22], as well as some minor amounts of Magneli phases (Ti_nO_{2n-1}; n=4 to 10).

Table II shows the porosity values obtained by SEM for all the coatings. Porosity data agree with the typical values observed in these types of coatings. However, some differences were also found between them. The coatings obtained from both commercial powders presented a lower porosity due to different reasons. On the one hand the fused nature and small grain size of the MC sample. On the other hand, NC sample contains higher amount of smaller granules. Indeed, smaller granules are easier to melt, giving rise to more deformable droplets, and consequently to lower coating porosity [3,18]. Although this last statement could be inconsistent with the fact that NC coating showed a higher amount of partially molten areas it should be taken into account that nano-scale porosity can hardly be evaluated by SEM technique. With regard to the feedstocks prepared in this work, thermal treatment results in coatings with slightly lower porosity, meanwhile no differences were observed between AsTn30 and AsTn50 powders. This is because, at this low range of coating porosities the contribution of the agglomerate density to the final coating porosity is negligible as compared with the contribution coming from the melting and subsequent deformation of the agglomerates during the deposition process. On the other hand, although some partially molten areas were identified by SEM these areas could not be quantified owing to their low proportion in the coating. Finally, coatings thicknesses are also detailed in table II. As it can be seen the lowest thickness was obtained with the commercial, fused and crushed feedstock.

3.4 Coating mechanical properties

Coatings mechanical properties (adhesion strength, Vickers microhardness, fracture toughness, and wear rate) for the four spray-dried feedstocks (untreated AsTn30 and AsTn50 and heat treated AsTn30-1200 ºC and AsTn50-1200 ºC) as well as for the two reference

coatings (MC and NC) are shown in figure 10 in terms of bar diagrams. As it can be seen, despite the differences in the characteristics of the feeding powders, the adhesion strength of all coatings showed similar values.

However, nanostructured coating (NC) showed somehow lower fracture toughness than that of conventional and submicron-nanometric ones. Such results are apparently in contradiction with the common hypothesis of a crack deviation effect of the unmelted nanozones present throughout the bimodal microstructure [18,19,21] suggesting poor cohesion of these nanozones due to the low density of the granules found in the corresponding feedstock together with the plasma spraying conditions used in this work. As a consequence, cracks may propagate easily between the nanoparticles explaining the lower fracture toughness. With regard to the rest of feedstocks, higher values of toughness were obtained for the coatings deposited from the spray-dried powders prepared in this research. These values were even higher than that of the MC coating. A much better microstructural homogeneity of these coatings as set out above in comparison with the one sprayed from the nanostructured feedstock as well as the presence of fewer but denser partially molten areas can be the reason for such high values of toughness.

More interestingly, significant differences were observed in the microhardness of the coatings, which varied from 2.2 GPa, for the conventional layer, up to 9.5 GPa, for AsTn30-1200 ºC coating. Besides, it can be observed that, when the microhardness increases, the wear resistance of the coating is improved. In fact, the best wear performance was found for AsTn30-1200 ºC coating while MC layer displayed the highest wear loss. Nanostructured coating (NC) shows an intermediate behaviour, with a significantly higher wear resistance than that of the conventional layer

The increased wear resistance of coatings obtained from nanostructured feedstocks in comparison with conventional (obtained from micrometric powders) coatings has been extensively reported in the recent literature [10,16,18,21]. The reasons showed in the literature for explaining this behaviour are as follows: the toughening contribution of the partially molten nanostructured zones [18,23,24] (not seen in this work), a more homogeneous TiO_2 distribution

inside the splats leading to higher splat bonding strength [5,16] and the role of different additives such as CeO_2 and ZrO_2 added to the composition [25]. In this mentioned research, the effect of agglomerate size and size distribution of the feedstock on the final coating microstructure has also been pointed out [18,26,27]. As reported elsewhere a feedstock with smaller agglomerates and a narrower agglomerate size distribution is preferred to produce dense coatings exhibiting well bonded, relatively dense nanostructured regions. All these works have focused on agglomerate size meanwhile the influence of the agglomerate density has been scarcely addressed. Bertrand et al [28] showed that the combination of dense powder with large agglomerate size produces coatings with very high amount of unmolten areas in TiO_2 coatings whenever low energy spraying conditions were used. In fact, calculations with zirconia powder [29] have proven that dense (5680 kg/m^3) zirconia agglomerates, 50 μm in diameter, melt much more than porous (2840 kg/m^3) due to the better heat propagation. Following all this research, in this work, we have shown that the use of high density spray-dried agglomerates in the feeding powder gives rise to low porosity coatings with a quite homogeneous microstructure leading to optimal mechanical properties. The way of obtaining such high density agglomerates was based on the use of a bimodal particle size distribution in the starting powder agglomerates with a significant amount of submicron-sized particles instead of nanosized ones. The employment of submicron-sized particles makes it easy the processability of the spray-drying suspension allowing the preparation of high solids content suspensions. Although the findings obtained have been very promising, further research is still necessary so as to connect feedstock characteristics and coating microstructure and properties by using the Al_2O_3-TiO_2 system and/or other plasma spray techniques.

4 Conclusions

This study compares the microstructure and mechanical properties of Al_2O_3-13 wt% TiO_2 APS coatings deposited from powders obtained by spray drying two starting suspensions of different solids content, prepared by adding nanosized TiO_2 and submicron-sized Al_2O_3 powders to water. The spray-dried granules were heat-treated to reduce their porosity. Thermal

treatment temperature was chosen on the basis of the sintering behaviour of the feedstocks. The powders were fully characterised in both untreated and thermally treated state. Comparison with a conventional (microstructured) and a nanostructured commercial feedstock was carried out.

Despite the differences observed in the powders studied, in general, all the samples exhibit adequate characteristics in terms of granule bulk density and powder flowability so as to be used as APS powders. In particular, the use of highly concentrated suspensions containing a bimodal distribution (submicron- and nano-sized particles) leads to a spray-dried powder with a highest agglomerate density and good flowability. Thermal treatment was shown to be an efficient process for producing highly sinterable feedstock, yielding coatings with slightly lower porosity, independently of solid concentration of the starting suspension used to obtain the reconstituted agglomerates.

All coatings, except the conventional one, displayed a bimodal microstructure with partially molten agglomerates that retained the initial nanostructure of the feedstock surrounded by a fully molten matrix. However, the amount of these partially molten areas is much higher in the case of the coating obtained from the nanostructured commercial powder which was constituted by highly porous agglomerates.

In general, the coatings obtained from the submicron–nanometric reconstituted powders led to better mechanical properties than those of the coating obtained from the nanostructured feedstock whereas the conventional coatings displayed the worst wear behaviour. A much better microstructural homogeneity of these coatings in comparison with the one sprayed from the nanostructured feedstock, a long with the presence of fewer but denser partially molten areas can be the reason for such enhanced values of mechanical properties, particularly microhardness and wear resistance. Although the findings obtained are very promising, further research is still necessary so as to connect feedstock characteristics and coating microstructure and properties in this or other ceramic systems.

Acknowledgements

This work has been supported by Spanish Ministry of Economy and Competitiveness (MAT2009-14144-C03-01 and -02).

References

[1] Faure B, Lindeløv JS, Wahlberg M, Adkins N, Jackson P, Bergström L. Spray drying of TiO_2 nanoparticles into redispersible granules. Powder Technol. 2010; 203(2): 384-8.

[2] Fauchais P, Montavon G, Lima RS, Marple BR. Engineering a new class of thermal spray nano-based microstructures from agglomerated nanostructured particles, suspensions and solutions: an invited review. J. Phys. D: Appl. Phys. 44 093001 doi:10.1088/0022-3727/44/9/093001.

[3] Fauchais P, Montavon G, Bertrand G. From Powders to Thermally Sprayed Coatings J. Therm. Spray Technol. 2010; 19(1-2): 56-80.

[4] Berger-Keller N, Bertrand G, Filiare C, Meunier C, Coddet C. Microstructure of plasma-sprayed titania coatings deposited from spray-dried powder. Surf. Coat. Technol. 2003; 168(2-3): 281-90.

[5] Ahn J, Hwang B, Song EP, Lee S, Kim NJ. Correlation of microstructure and wear resistance of Al_2O_3-TiO_2 coatings plasma sprayed with nanopowders. Metall. Mater. Trans. A 2006; 37(6): 1851-61.

[6] Lin X, Zeng Y, Lee SW, Ding C. Characterization of alumina–3 wt.% titania coating prepared by plasma spraying of nanostructured powders. J. Eur. Ceram. Soc. 2004; 24(4): 627-34.

[7] Fauchais P, Vardelle M, Coudert JF, Vardelle A, Delbos C, Fazilleau J. Thermal plasma deposition from thick to thin coatings and from micro- to nanostructure. Pure Appl. Chem. 2005; 77(2): 475-85.

[8] Darut G, Ageorges H, Denoirjean A, Montavon G, Fauchais P. Effect of the structural scale of plasma-sprayed alumina coatings on their friction coefficients. J. Therm. Spray Technol. 2008; 17(5-6): 788-95.

[9] Molina T, Vicent M, Sánchez E, Moreno R. Dispersion and reaction sintering of alumina–titania mixtures. Mater. Res. Bull. 2012; 47: 2469-74.

[10] Vicent M et al. Influence of the feedstock characteristics on the microstructure and properties of Al_2O_3–TiO_2 plasma-sprayed coatings. Surf. Coat. Technol. 2013; 220: 74-9.

[11] Sánchez E et al. Preparation and spray drying of Al_2O_3–TiO_2 nanoparticle suspensions to obtain nanostructured coatings by APS. Surf. Coat. Technol. 2010; 205(4): 987-92.

[12] Bordes MC et al. Microstructure and photocatalytic activity of APS coatings obtained from different TiO_2 nanopowders. Surf. Coat. Technol. 2013; 220: 179-86.

[13] Vicent M, Sánchez E, Santacruz I, Moreno R. Dispersion of TiO_2 nanopowders to obtain homogeneous nanostructured granules by spray-drying J. Eur. Ceram. Soc. 2011; 31(8): 1413-9.

[14] Gutiérrez CA, Moreno R. Preventing ageing on Al_2O_3 casting slips dispersed with polyelectrolytes. J. Mater. Sci. 2000; 35(23): 5867-72.

[15] Amorós JL, Blasco A, Enrique JE, Negre F. Características de polvos cerámicos para prensado (Characteristics of ceramic powders for pressing). Bol. Soc. Esp. Ceram. Vidr. 1987; 26(1): 31-7.

[16] Sánchez E et al. Deposition of Al_2O_3-TiO_2 nanostructured powders by atmospheric plasma spraying J. Therm. Spray Technol. 2008; 17(3): 329-37.

[17] Cao XQ, Vassen R, Schwartz S, Jungen W, Tietz F, Stöever D. Spray-drying of ceramics for plasma-spray coating. J. Eur. Ceram. Soc. 2000; 20(14-15): 2433-9.

[18] Marple BR, Lima RS. Engineering nanostructured thermal spray coatings: process-property-performance relationships of ceramic based materials. Adv. Appl. Ceram. 2007; 106(5): 265-75.

[19] Lima RS, Marple BR. Thermal spray coatings engineered from nanostructured ceramic agglomerated powders for structural, thermal barrier and biomedical applications: A Review. J. Therm. Spray Technol. 2007; 16(1): 40-63.

[20] Bansal P, Padture NP, Vasiliev A. Improved interfacial mechanical properties of Al_2O_3-13wt%TiO_2 plasma-sprayed coatings derived from nanocrystalline powders. Acta Mater. 2003; 51(10): 2959-70.

[21] Dejang N, Watcharapasorn A, Wirojupatump S, Niranatlumpong P, Jiansirisomboon S. Fabrication and properties of plasma-sprayed Al_2O_3/TiO_2 composite coatings: A role of nano-sized TiO_2 addition. Surf. Coat. Tech. 2010; 204(9-10): 1651-7.

[22] YangY, Wang Y, Wang Z, Liu G, Tian W. Preparation and sintering behaviour of nanostructured alumina/titania composite powders modified with nano-dopants. Mat. Sci. Eng. A. 2008; 490(1-2): 457-64.

[23] Luo H, Goberman D, Shaw L, Gell M. Indentation fracture behavior of plasma-sprayed nanostructured Al_2O_3–13wt.%TiO_2 coatings. Mat. Sci. Eng. A. 2003; 346(1-2): 237-45.

[24] Song EP, Ahn J, Lee S, Kim NJ. Effects of critical plasma spray parameter and spray distance on wear resistance of Al_2O_3–8wt.%TiO_2 coatings plasma-sprayed with nanopowders. Surf. Coat. Technol. 2008; 202(15): 3625-32.

[25] Wang Y, Jiang S, Wang M, Wang S, Xiao TD, Strutt PR. Abrasive wear characteristics of plasma sprayed nanostructured alumina/titania coatings. Wear 2000; 237(2): 176-85.

[26] Lima RS, Kucuk A, Berndt CC. Integrity of nanostructured partially stabilized zirconia after plasma spray processing. Mat. Sci. Eng. A. 2001; 313(1-2): 75-82.

[27] Guo HB, Murakami H, Kuroda S. Effect of hollow spherical powder size distribution on porosity and segmentation cracks in thermal barrier coatings. J. Amer. Ceram. Soc. 2006; 89(12): 3797-3804.

[28] Bertrand G, Berger-Keller N, Meunier C, Coddet C. Evaluation of metastable phase and microhardness on plasma sprayed titania coatings. Surf. Coat. Technol. 2006; 200(16-17): 5013-9.

[29] Ben-Ettouil F, Mazhorova O, Pateyron B, Ageorges H, El-Ganaoui M, Fauchais P. Predicting dynamic and thermal histories of agglomerated particles injected within a d.c. plasma jet. Surf. Coat. Technol. 2008; 202(18): 4491-5.

Figure captions

Figure 1. FEG-ESEM micrographs of the as spray-dried powders obtained from 30 vol.% and 50 vol.% suspensions at different magnifications (samples AsTn30 and AsTn50 respectively)

Figure 2. Shrinkage versus temperature curves for samples AsTn30 and AsTn50 together with the reference NC powder obtained by means of the hot stage microscope

Figure 3. FEG-ESEM micrographs of AsTn30 and AsTn50 spray-dried powders thermally-treated at two temperatures

Figure 4. Pore size distribution curves obtained by mercury intrusion porosimetry for AsTn30 and AsTn50 powders thermally untreated and thermally treated at 1235 ºC

Figure 5. Granule size distribution of the thermally treated spray-dried powders obtained from 30 vol.% and 50 vol.% suspensions (samples AsTn30-1200 ºC and AsTn50-1200 ºC respectively)

Figure 6. XRD patterns for AsTn50 powder untreated and thermally treated at 1200 ºC

Figure 7. SEM micrographs of AsTn30, AsTn50, AsTn30-1200 ºC and AsTn50-1200 ºC powders together with two representative micrographs of reference coatings (MC and NC) obtained with the same spraying conditions

Figure 8. Comparison of higher magnification micrographs of the partially molten areas in NC and AsTn50-1200 ºC coatings

Figure 9. XRD patterns of coatings obtained from a) AsTn30 and AsTn30-1200 ºC powders, b) AsTn50 and AsTn50-1200 ºC powders

Figure 10. Mechanical properties of all the coatings studied

Tables

Table I. Main powder characteristics of all feedstocks studied in this work

Feedstock characteristic	AsTn30	AsTn50	AsTn30-1200 ºC	AsTn50-1200 ºC	MC	NC
Volumetric mean size (µm)	---(*)	---(*)	57	110	36	38
Granule bulk density (kg/m^3)	2510±15	2780±20	3100±20	3580±30	3830±15	1730±15
Hausner ratio	1.18±0.03	1.16±0.03	1.25±0.03	1.18±0.04	1.28±0.04	1.19±0.03

(*) Granule size distribution could not be measured by laser diffraction but FEG-ESEM micrographs confirm similar size in thermally untreated and in heat-treated powders

Table II. Microstructural features of the coatings obtained from reconstituted powders both untreated and heat treated as well as from the reference feedstocks

	AsTn30	AsTn50	AsTn30-1200 ºC	AsTn50-1200 ºC	MC	NC
Porosity (%)	8	7	5	5	3	3
Thickness (µm)	173±16	213±34	173±30	170±25	52±14	103±14

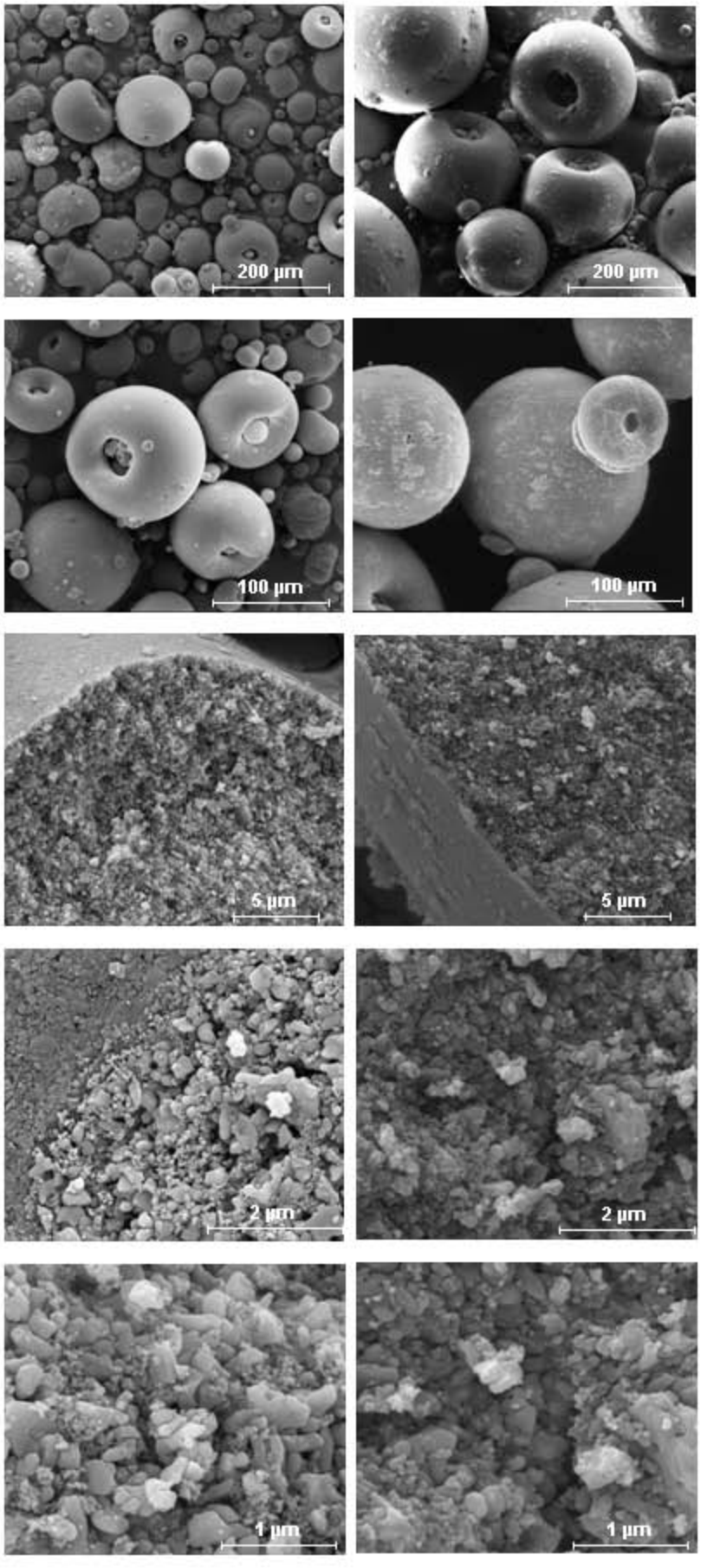
200 µm
200 µm
100 µm
100 µm
5 µm
5 µm
2 µm
2 µm
1 µm
1 µm

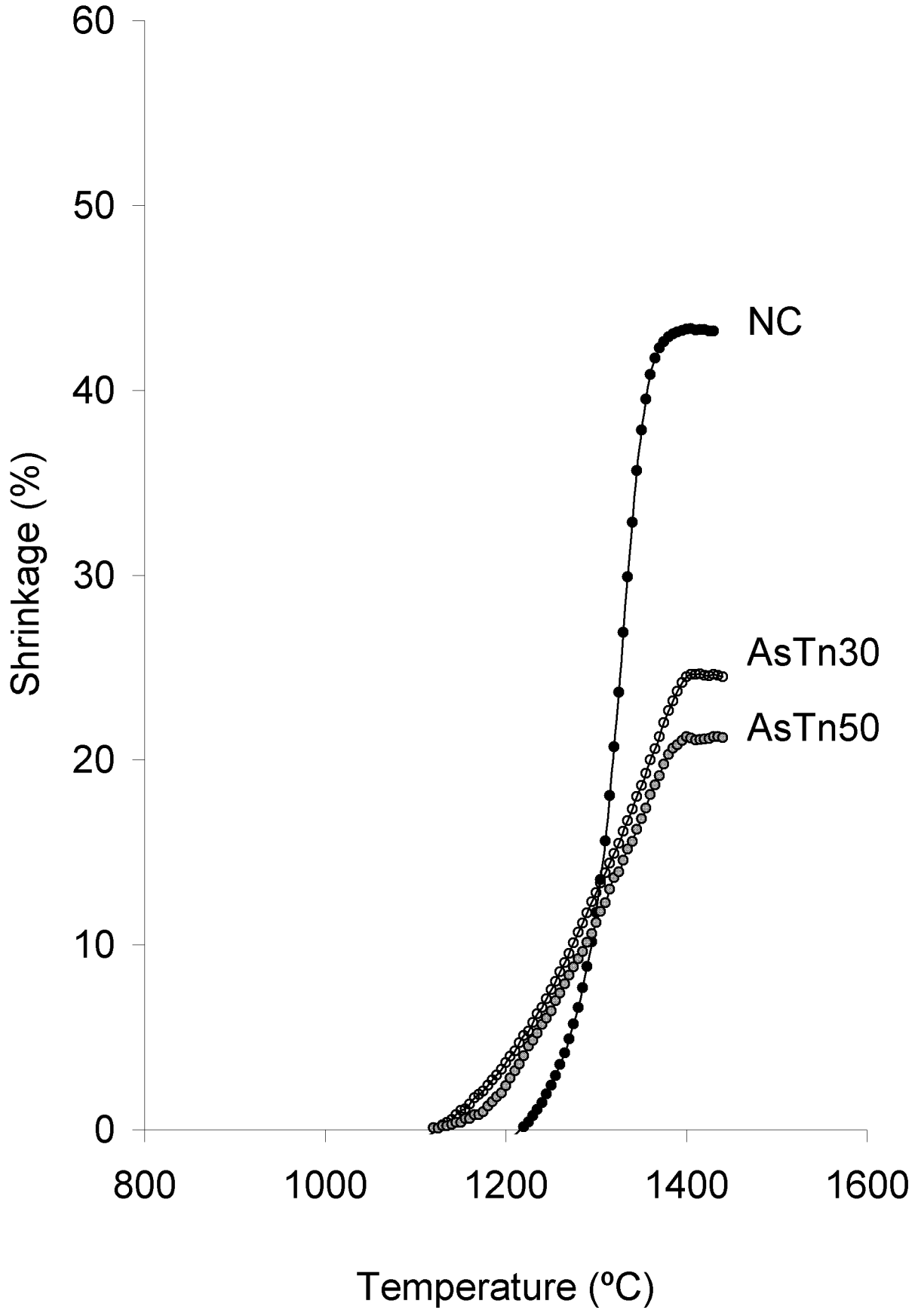
60
50
40
30
20
10
0
Shrinkage (%)
800
1000
1200
1400
1600
Temperature (ºC)
NC
AsTn30
AsTn50

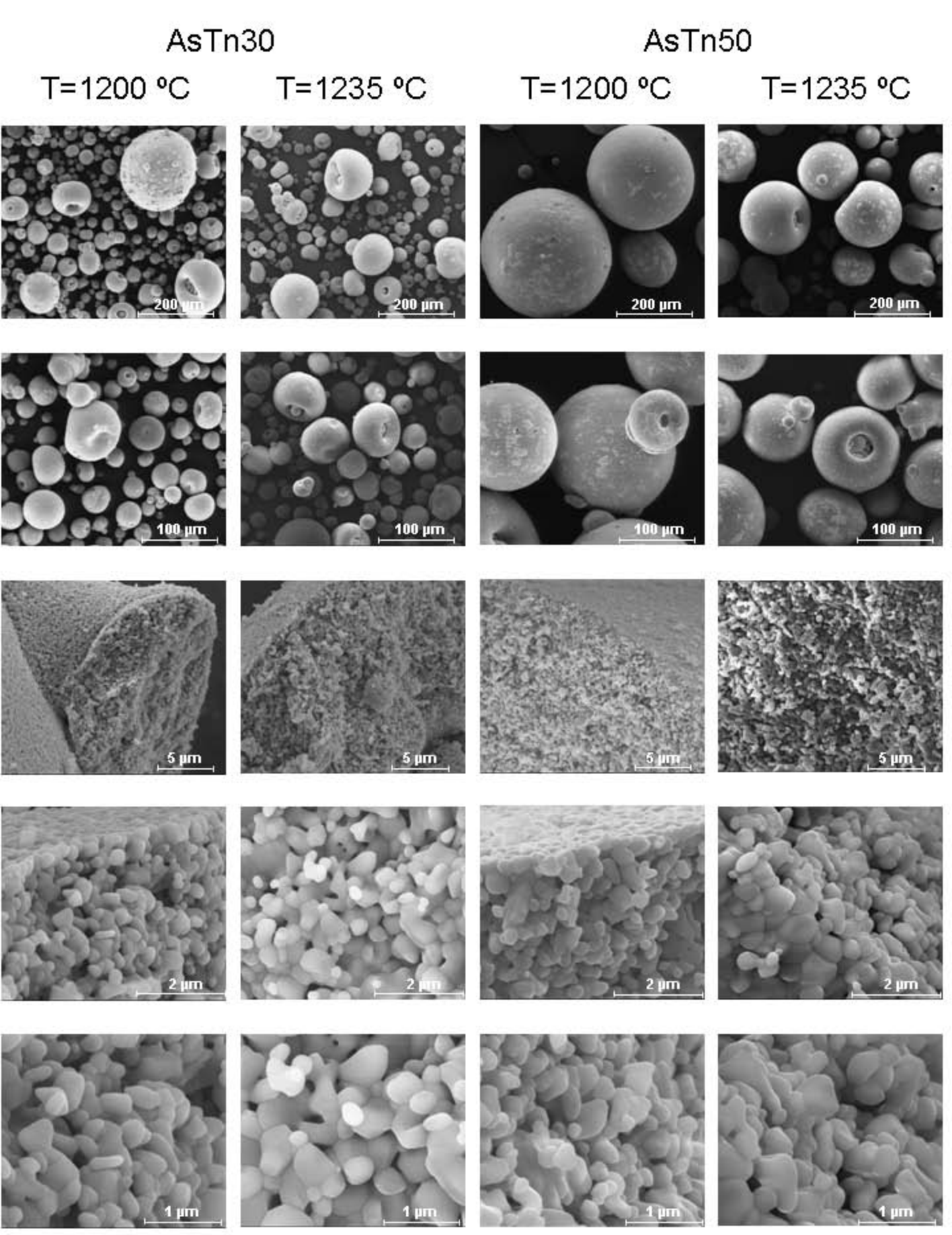
AsTn30
AsTn50
T=1200 ºC
T=1235 ºC
T=1200 ºC
T=1235 ºC
200 µm
100 µm
5 µm
2 µm
1 µm

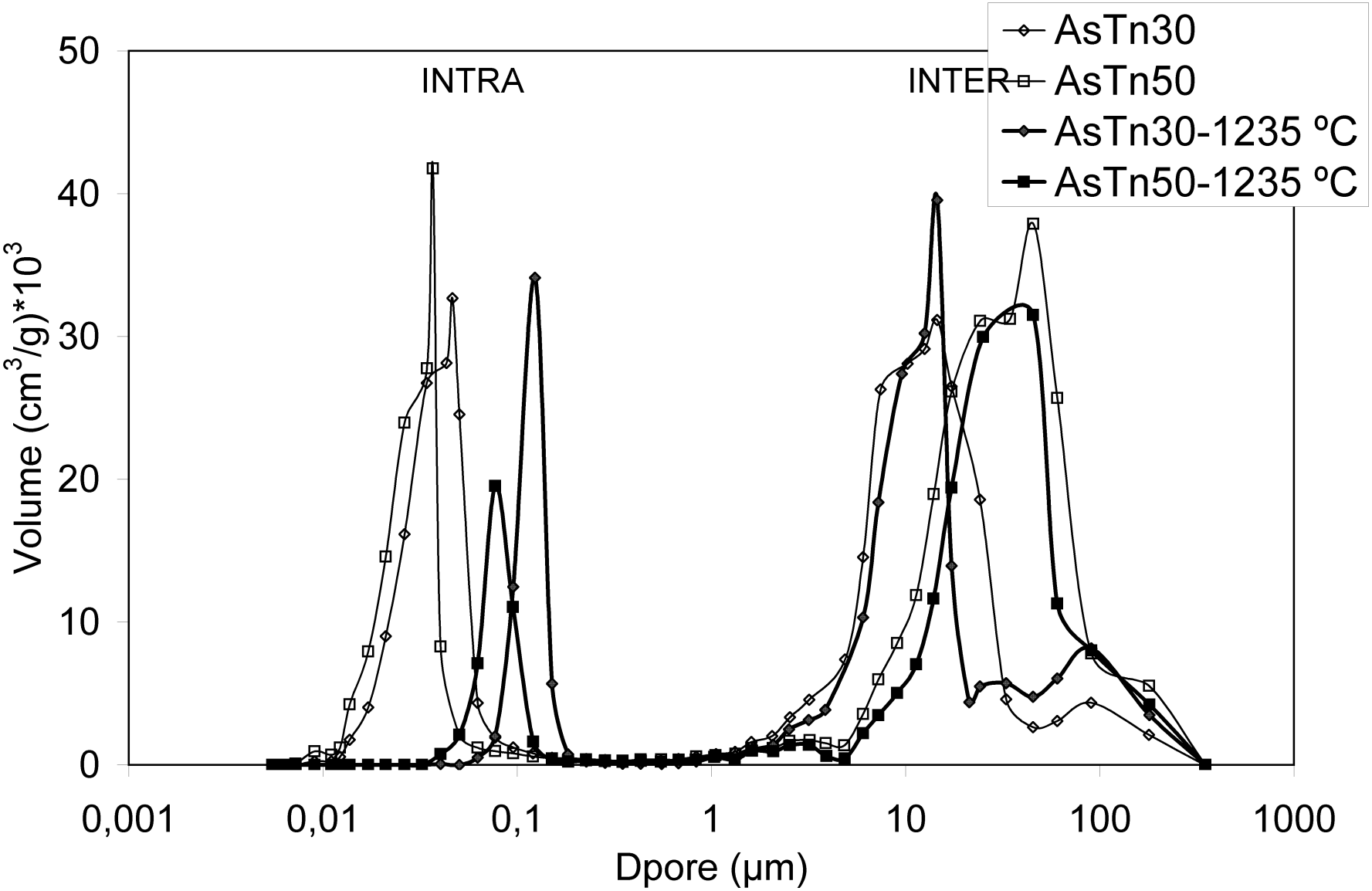
AsTn30
AsTn50
AsTn30-1235 ºC
AsTn50-1235 ºC
INTRA
INTER
Volume (cm3/g)*10^3
Dpore (µm)
0
10
20
30
40
50
0,001
0,01
0,1
1
10
100
1000

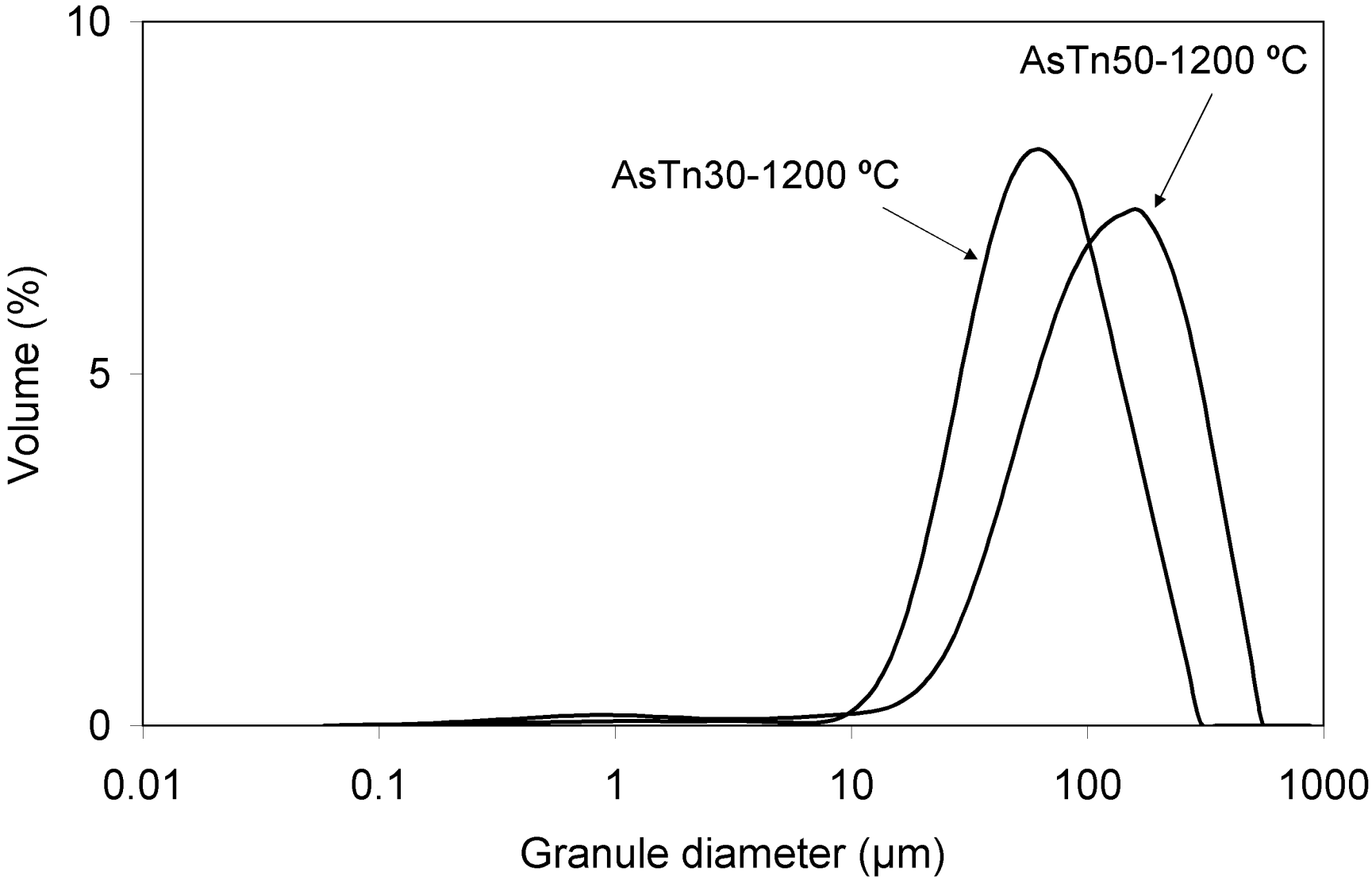
10
5
0
Volume (%)
AsTn50-1200 ºC
AsTn30-1200 ºC
0.01
0.1
1
10
100
1000
Granule diameter (µm)

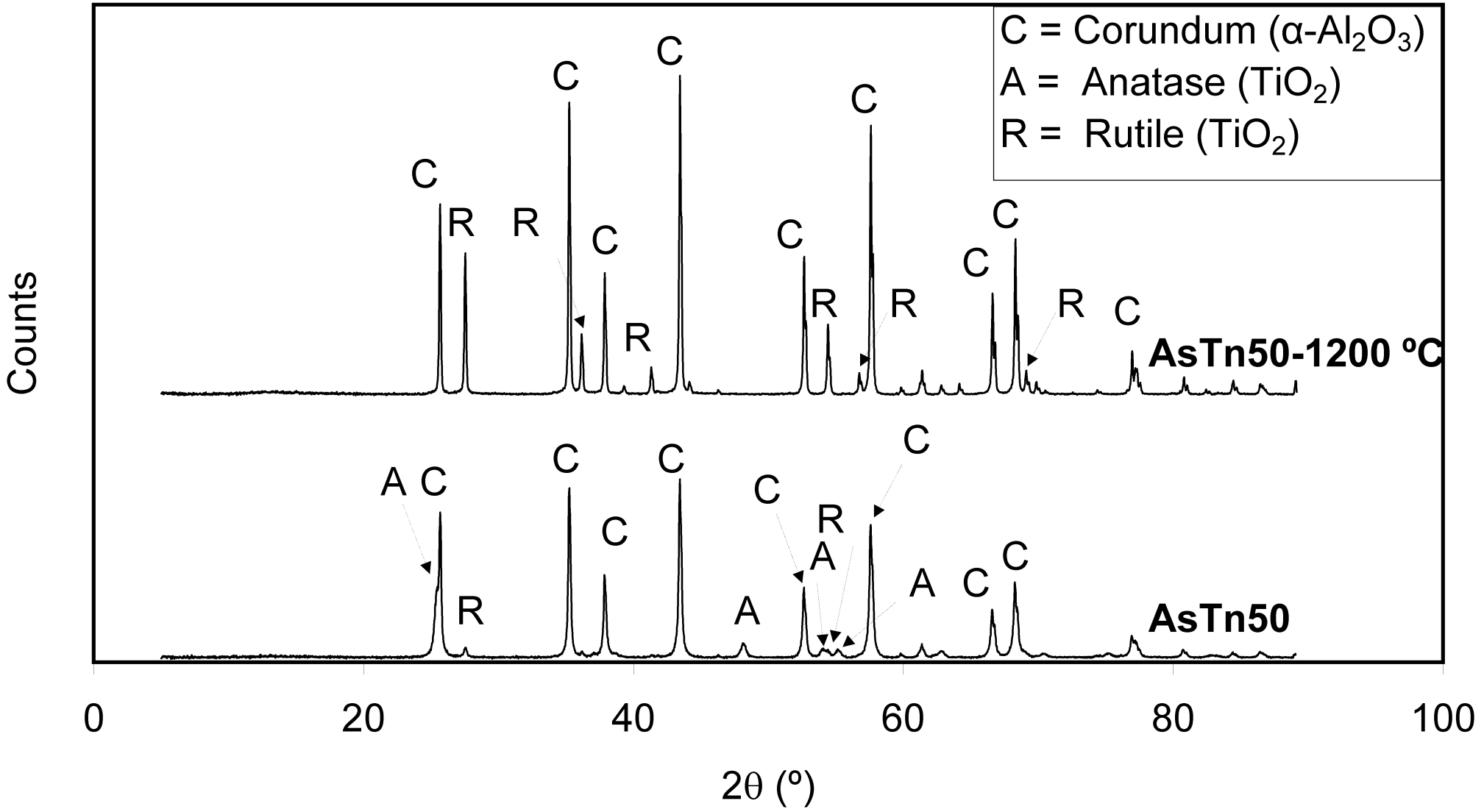
C = Corundum (α-Al2O3)
A = Anatase (TiO2)
R = Rutile (TiO2)
AsTn50-1200 ºC
AsTn50
Counts
2θ (º)
0
20
40
60
80
100

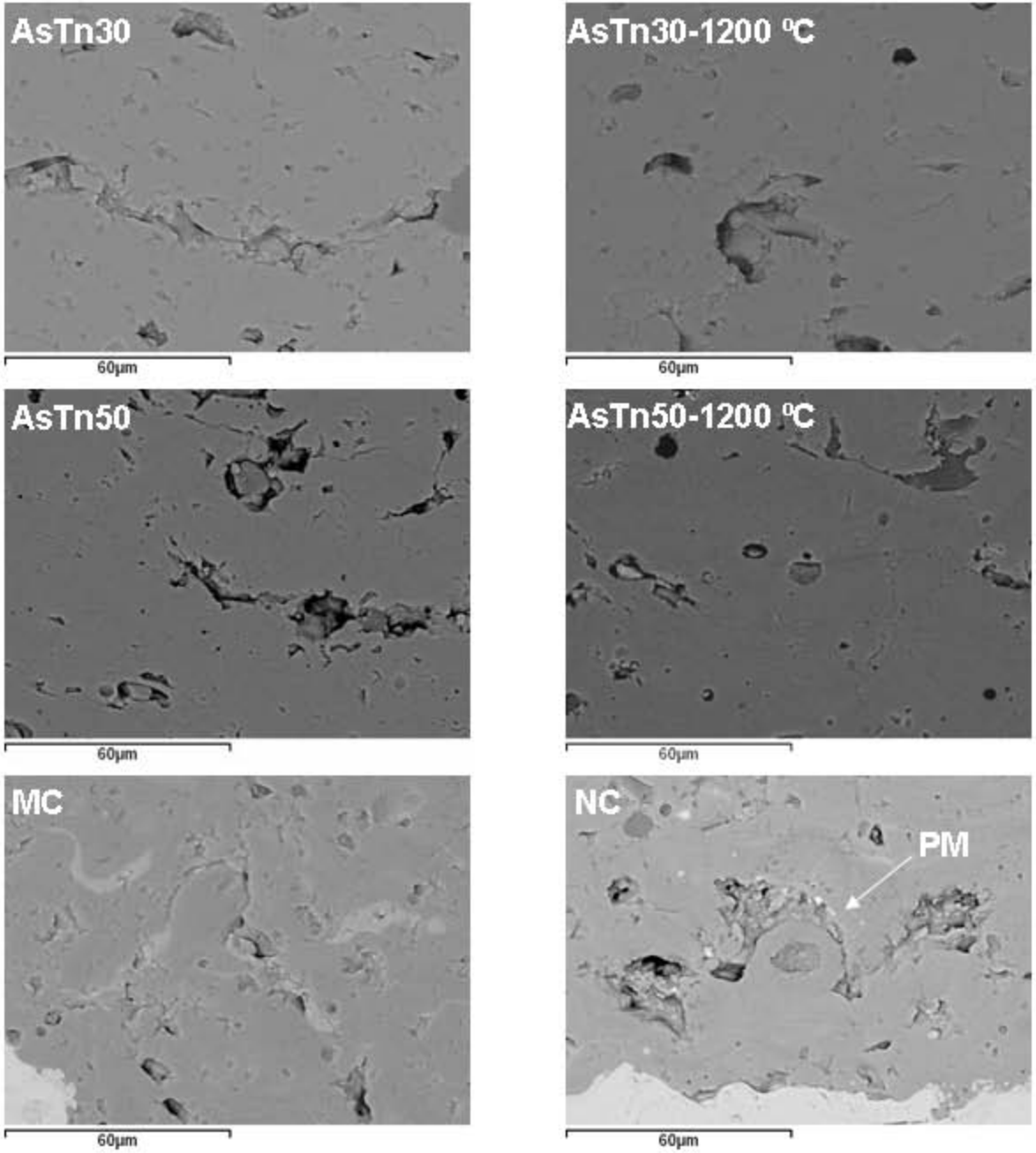
AsTn30
60µm
AsTn30-1200 °C
60µm
AsTn50
60µm
AsTn50-1200 °C
60µm
MC
60µm
NC
PM
60µm

AsTn30-1200 ºC

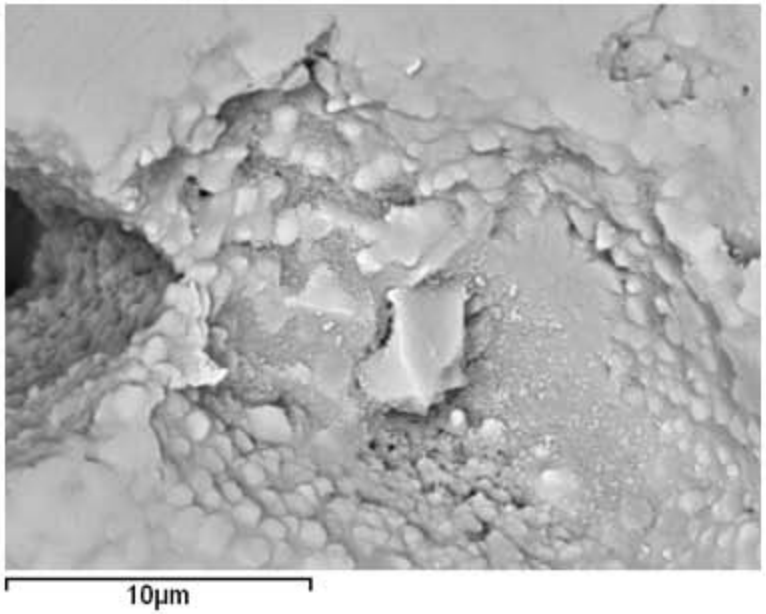

NC

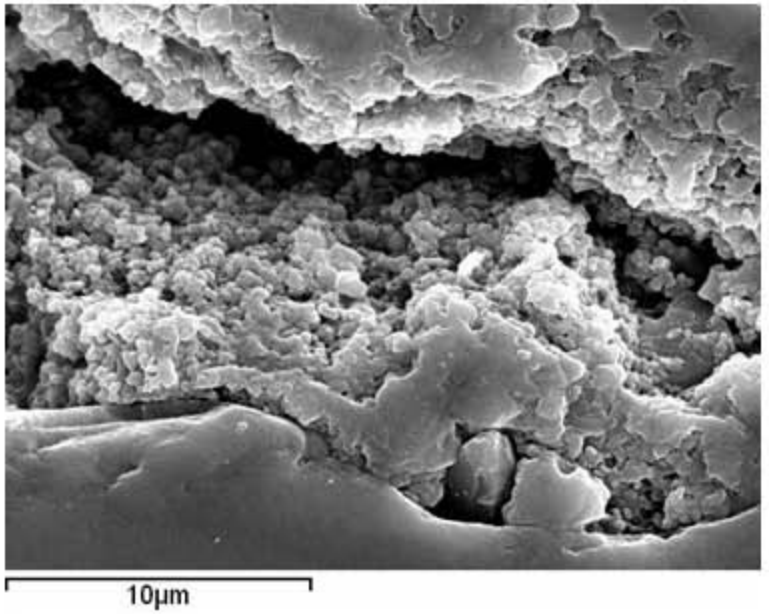

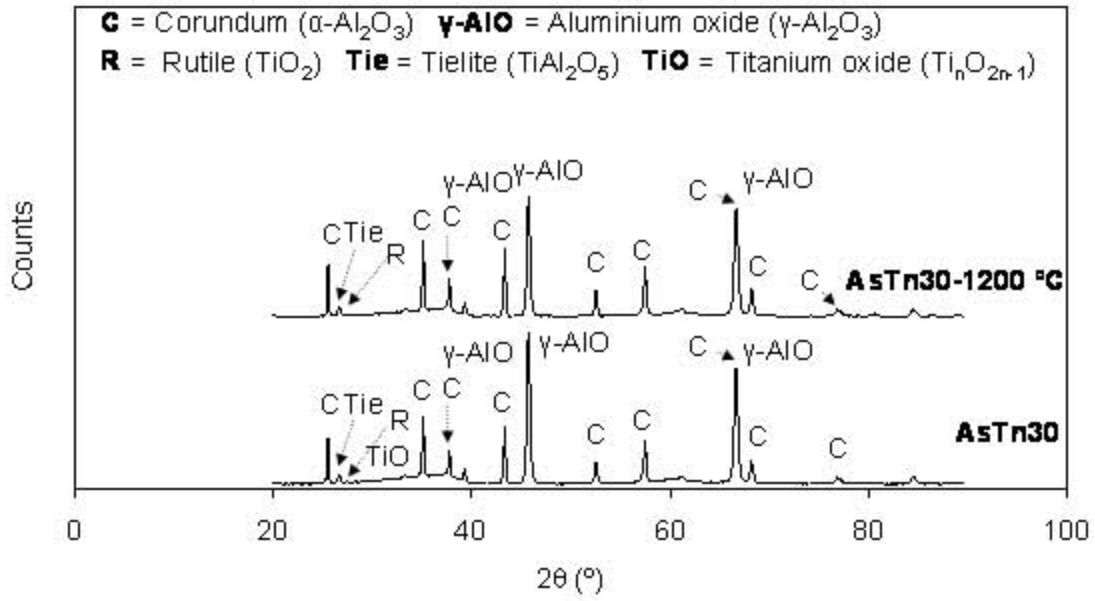
C = Corundum (α-Al2O3) γ-AlO = Aluminium oxide (γ-Al2O3)
R = Rutile (TiO2) Tie = Tielite (TiAl2O5) TiO = Titanium oxide (TinO2n-1)
Counts
AsTn30-1200 °C
AsTn30
0
20
40
60
80
100
2θ (°)

a)

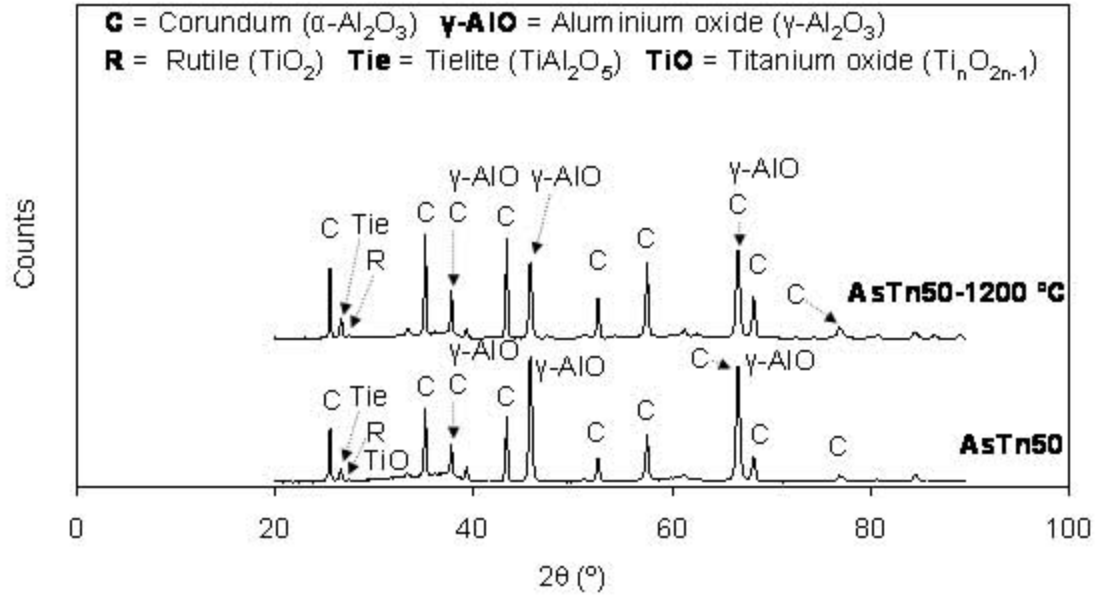
C = Corundum (α-Al2O3) γ-AlO = Aluminium oxide (γ-Al2O3)
R = Rutile (TiO2) Tie = Tielite (TiAl2O5) TiO = Titanium oxide (TinO2n-1)
Counts
AsTn50-1200 °C
AsTn50
0
20
40
60
80
100
2θ (°)

b)

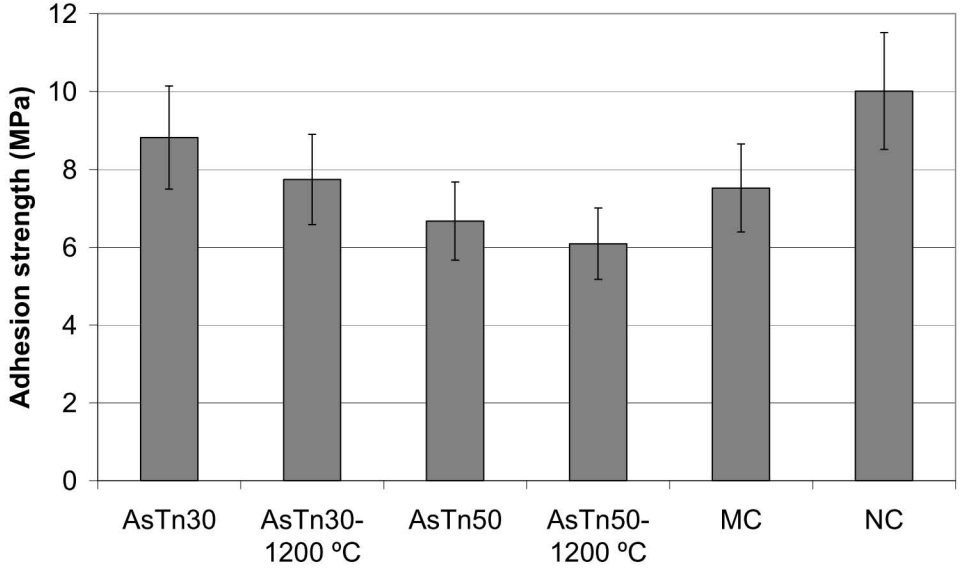
Adhesion strength (MPa)
0
2
4
6
8
10
12
AsTn30
AsTn30-1200 ºC
AsTn50
AsTn50-1200 ºC
MC
NC

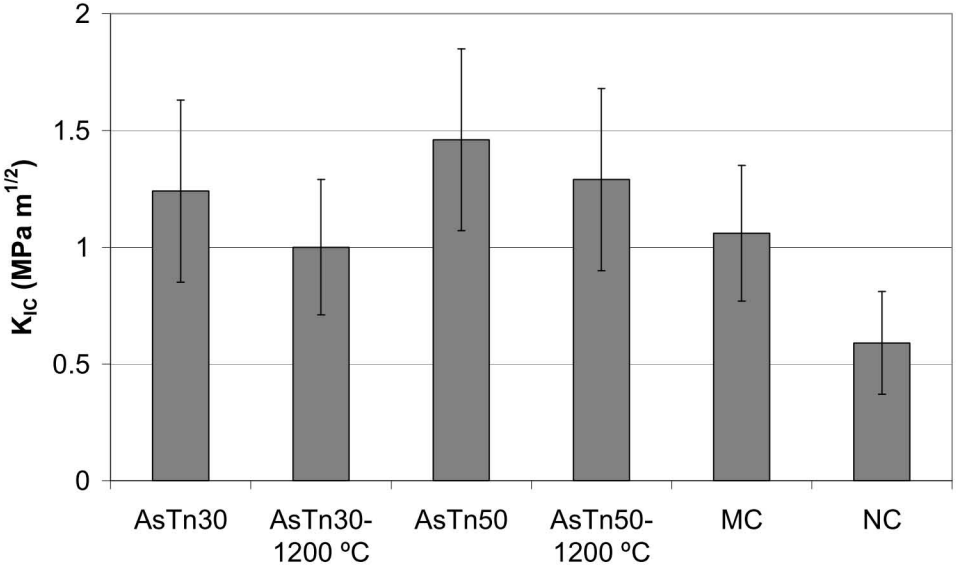
K_{IC} (MPa $m^{1/2}$)
0
0.5
1
1.5
2
AsTn30
AsTn30-1200 ºC
AsTn50
AsTn50-1200 ºC
MC
NC

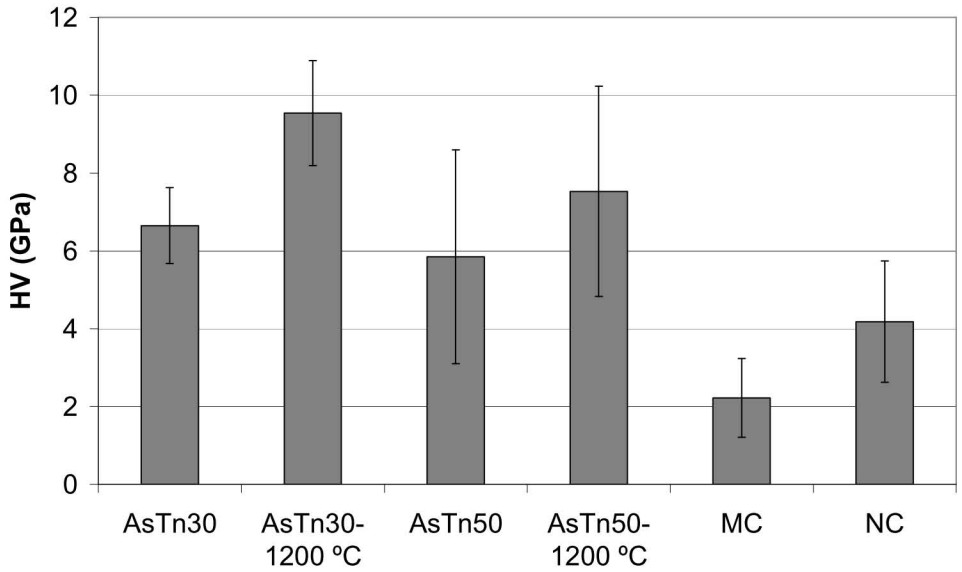
HV (GPa)
0
2
4
6
8
10
12
AsTn30
AsTn30-1200 ºC
AsTn50
AsTn50-1200 ºC
MC
NC

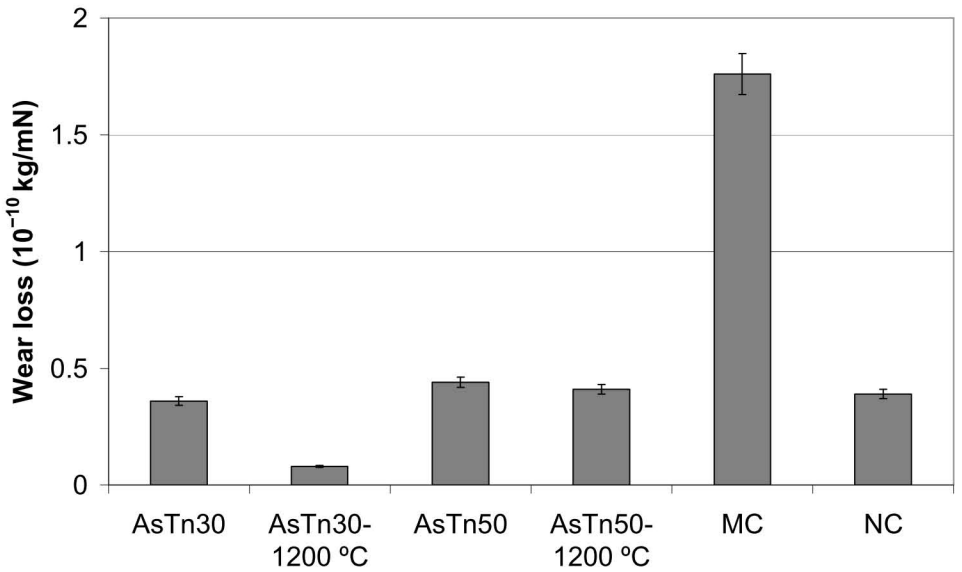
Wear loss (10^{-10} kg/mN)
0
0.5
1
1.5
2
AsTn30
AsTn30-1200 ºC
AsTn50
AsTn50-1200 ºC
MC
NC